chemosensors

MDPI

Article

Development of Novel and Highly Specific ssDNA-Aptamer-Based Electrochemical Biosensor for Rapid Detection of Mercury (II) and Lead (II) Ions in Water

Hisham Abu-Ali [1,2,*], Alexei Nabok [1] and Thomas J. Smith [3]

[1] Material and Engineering Research Institute, Sheffield Hallam University, Sheffield S1 1WB, UK; a.nabok@shu.ac.uk
[2] Faculty of Science, University of Basrah, Basrah 61004, Iraq
[3] Biomolecular Research Centre, Sheffield Hallam University, Sheffield S1 1WB, UK; scitjs@exchange.shu.ac.uk
* Correspondence: b4039024@my.shu.ac.uk

Received: 21 March 2019; Accepted: 28 May 2019; Published: 4 June 2019

Abstract: In this work, we report on the development of an electrochemical biosensor for high selectivity and rapid detection of Hg^{2+} and Pb^{2+} ions using DNA-based specific aptamer probes labeled with ferrocene (or methylene blue) and thiol groups at their 5′ and 3′ termini, respectively. Aptamers were immobilized onto the surface of screen-printed gold electrodes via the SH (thiol) groups, and then cyclic voltammetry and impedance spectra measurements were performed in buffer solutions with the addition of $HgCl_2$ and $PbCl_2$ salts at different concentrations. Changes in 3D conformation of aptamers, caused by binding their respective targets, e.g., Hg^{2+} and Pb^{2+} ions, were accompanied by an increase in the electron transfer between the redox label and the electrode. Accordingly, the presence of the above ions can be detected electrochemically. The detection of Hg^{2+} and Pb^{2+} ions in a wide range of concentrations as low as 0.1 ng/mL (or 0.1 ppb) was achieved. The study of the kinetics of aptamer/heavy metal ions binding gave the values of the affinity constants of approximately 9.10^{-7} mol, which proved the high specificity of the aptamers used.

Keywords: aptamer sensors; electrochemical sensors; heavy metal ions; cyclic voltammetry; impedance spectroscopy; binding kinetics

1. Introduction

The detection of toxic metal ions in aquatic environment is an important global issue because these contaminants may have severe effects on plants, animals, and humans as well as on ecosystem [1]. Among the most toxic metallic water pollutants in aquatic environments are mercury and lead [2]. Lead can cause renal malfunction and can inhibit brain development in humans [3]; mercury can cause damage of the brain, heart, and kidneys [4]. The detection of heavy metals in low concentrations is a difficult task; however, it can be achieved with existing advanced analytical methods, such as atomic absorption or atomic emission spectroscopies (AAS, AES), inductively coupled plasma mass spectroscopy (ICP-MS), cold vapor atomic fluorescence spectroscopy (CVAFS), and high-performance liquid chromatography (HPLC) [5]. These methods are extremely sensitive but expensive and require specialized laboratory conditions and highly trained personnel. As a result, both the time and cost of the analysis are very high.

An alternative approach uses biosensors, which can be much simpler and less expensive [6]. Biosensors require bioreceptors that specifically recognise and bind target analyte molecules. Typical natural bio-receptors used in biosensors, e.g., enzymes and antibodies, are highly specific and, in many

instances, easily provide such functionality. Synthetic bio-receptors, such as aptamers, have become very popular recently and provide similar functionality. A wide variety of aptamers offer both an additional and versatile way of providing the specific interactions required for biosensors. Recently, great progress has been made in the development of optical and electrochemical techniques for the detection of toxic metal ions using either artificial receptors, e.g., nanoparticles functionalised with DNAzymes [7], graphene oxide chemiresistor [8], or natural biological objects such as bacteria [9] and whole cells [10,11].

Aptamers show high affinity towards a wide range of target analytes, including proteins, metal ions, and pathogenic microorganisms. Aptamers can bind their targets with comparable affinity and specificity to antibodies; they also possess several advantages such as accurate and reproducible chemical synthesis [12]. Aptamers can be easily modified with new functional groups without affecting their activity. Numerous aptamer-based biosensors have been developed for the detection of a wide range of targets [13]. Many aptamers have been developed for the detection of low molecular weight pollutants in aquatic environments, for example, DNA-based aptamers specifically used for pesticides and mycotoxins [14,15] as well as for microcystin, antibiotics, and endocrine-disturbing chemicals [16]. Most aptamers are known to fold into their unique three-dimensional conformation upon binding the target, a process also described as "wrapping around" the target molecules. This change in conformation provides great flexibility for designing electrochemical apta-sensors [17], particularly suitable for the detection of small molecules. If the aptamers are labeled with redox groups, such as ferrocene or methylene blue, and then immobilized on an electrode surface [18], the changes in aptamer conformation upon binding the analyte reduce the distance between the redox tag and the electrode, and thus increase the electron transfer. The exploration of novel approaches and methodologies, such as the amplification of apta-sensor responses, are required for the detection of small molecules. Several methods for signal amplification have been demonstrated, such as a rolling circle amplification of the aptamer triggered by analyte binding [19], strand displacement amplification [20], as well as the use of labeled aptamers multiple redox active labels that can be enzymatically detected [21]. Aptamer-functionalized nanoparticles have also been reported for signal amplification in apta-sensors [22].

With regard to the detection of heavy metal ions, different types of aptamers have been developed, such as the T-rich aptamer, which forms a hairpin structure and binds several Hg ions [23]. Currently, the use of aptamers labelled with either fluorescent or redox groups is very common [24]. Previously, DNA-based aptamers containing TOTO-3 dye were designed to accommodate either Hg^{2+} ions via interaction with T-T sequences or Pb^{2+} with G-G sequences in their respective polynucleotide chains [25]. The T-Hg^{2+}-T complex formed due to the imino protons of the thymine nucleotide, which transposed with Hg^{2+}ions [26]. The interaction of these two aptamers with their respective targets induces conformational changes in the polynucleotide chains (from linear to a folded structure), which, in turn, affects the fluorescence of TOTO-3, i.e., the fluorescence intensity is reduced due to quenching when the label is in proximity to the surface of gold nanoparticle. Recently, an electrochemical aptasensor, based on (T-Hg^{2+}-T) coordination chemistry and nanoporous gold (NPG) for signal amplification, was designed for sensitive and selective detection of mercury ions Hg^{2+} in water [27]. Similarly, the anti-Pb aptamer, labelled with Cy5 fluorescent dye and immobilized on the surface of carbon nanotube, changed its conformation to G-quadruplex upon binding Pb^{2+} ions, thus bringing the label closer to the carbon nanotube, which acted as fluorescence quencher [28]. Another Pb^{2+} aptasensor, based on G-quadruplex structure, was constructed on graphene support functionalized with thionine [29].

In this paper, we used aptamers against Hg^{2+} and Pb^{2+} with nucleotide sequences similar to those reported in [30,31] but functionalized with electrochemically active labels of ferrocene and methylene blue, respectively, at 5′ termini. The sensing mechanism of these aptamer probes was based on the changes in the DNA strand's conformation from the linear to folded structures upon binding the respective metal ions, which affected the electron transfer between the redox label and the metal electrode.

2. Experimental Methodology

2.1. Aptamers and Other Chemicals

The following modified deoxy ribonucleotides (P1 and P2) selected as specific aptamers for Hg^{2+} and Pb^{2+} ions, respectively, were purchased from Sangon-Biotech (Shanghai, China):

P1: Ferrocene-**5′-TTCTTTCTT-CCCC-TTCTTTCTT-3′**-SH, [30].
P2: Methylene blue-**5′-CAACGGTTGGTGTGGTTGG-3′**-SH, [31].

The thiol groups (-SH) at the C3 termini were designed to provide strong and oriented binding of the aptamers to screen-printed gold electrodes. The redox functional groups, e.g., ferrocene or methylene blue, were attached to C5 termini to provide distinctive electrochemical properties, such as current peaks on CV characteristics associated with oxidation and reduction reactions.

The other chemicals used (all from Sigma Aldrich) were Hepes and phosphate-binding buffers (HBB and PBB), and 1,4-dithiothreitol (DTT). Hepes binding buffer (HBB) was prepared by dissolving 50 mM Hepes sodium salt, 3 mM $MgCl_2$, 120 mM NaCl, and 5 mM KCl in deionized Milli-Q water. The pH of the buffer was adjusted to 7.4. Similarly, phosphate-binding buffer (PBB) was prepared by dissolving 10 mM Na_2HPO_4, 1.76 mM KH_2PO_4, 3 mM $MgCl_2$, 2.7 mM KCl, and 137 mM NaCl. The pH of the buffer was adjusted to 7.4. The addition of $MgCl_2$ to the buffers was essential to preserve the secondary structure of aptamer from self-coiling. For long-term storage, as-received aptamer was prepared in sterilized, deionized water at 100 μM and stored at −20 °C in small aliquots.

2.2. Immobilization of Aptamers

The aptamers were immobilized on a gold surface via thiol groups at the 3′-termini according to the following procedure. Stock solution of the required aptamer was diluted to 1 μM with HBB or PBB supplemented with 1 mM of 1,4-dithiothretiol (DTT) and 3 mM of $MgCl_2$. DTT led to the removal of the protecting group from the SH moiety and released the aptamers with free SH end groups that could then bind to the surface of screen-printed gold electrode. Before immobilization, the aptamers solution samples were activated by rapid (1 min) heating up to 95 °C followed by 1 min cooling at 4 °C using a conventional thermocycler polymerase chain reaction unit (TECHNE PCR, version TC-3000). Following the procedure described in [32], the immobilization of aptamers was carried out by casting aptamers solution onto the screen-printed gold electrode surface; the samples were then incubated for 4 h at room temperature in a humidity chamber. The unreacted aptamers were removed from the electrode surface by several rinses with non-folding buffer (HBB), then the screen-printed gold electrode with immobilized aptamers was kept in HBB to prevent aptamers from coiling.

2.3. Electrochemical Measurements

All CV electrochemical measurements were carried out on a DropSTAT4000P potentiostat instrument (from DropSens) controlled by Autolab software using DropSens screen-printed gold electrodes (SPGEs). The electrodes have a conventional three electrode configuration with gold working and counter electrodes and a Ag/AgCl pseudo-reference electrode. CV measurements were carried out on electrodes with the immobilized aptamers, firstly, in pure buffer solution (HBB or PBB), then in buffer solutions with the addition of either $HgCl_2$ or $PbCl_2$ salts in different concentrations starting from 0.1 ng/mL up to 1μg/mL. Because the addition of heavy metal salts increased the conductivity of buffer solutions, control measurements were carried out on electrodes without aptamers at each concentration of metal salts.

The voltage range between −0.5 and +0.5 V was selected for these measurements to observe the characteristic peaks of both redox labels, e.g., ferrocene and methylene blue. The labels used have different redox potentials: 0.01 V for methylene blue, and 0.4 V for ferrocene. The selection of fixed voltage at ±0.2 V for further analysis allowed for observation of both the oxidation and reduction currents peaks, given their 0.2 V expansion on both sides. The aptamer/metal ions binding kinetics

at different concentrations of metal chlorides was studied by recording current in SPGEs at fixed potentials: −0.2 V for $HgCl_2$ and −0.4 V for $PbCl_2$.

The real samples of water taken from different natural resources in the area were tested using the same screen-printed electrodes with immobilized aptamers. The reference in this case was bottled drinking water.

Impedance spectra were measured using an impedance spectroscopy instrument 4000 A and gold interdigitated electrodes (from Metrohm DropSens) containing 250 fringes on each side spaced by 5µm; the overlapping length was 6.76 mm. The AC voltage amplitude was 5 mV with a frequency that varied from 100 mHz to100 kHz; no DC bias was applied. Similarly to CVs, the impedance spectra measurements were carried out on electrodes both coated and non-coated with aptamers in buffer solutions containing different concentrations of metal salts.

2.4. ICP-MS Measurements

In addition to electrochemical measurements, control measurements were carried out using PerkinElmer NexION^{TM} 350X ICP mass spectrometer to determine traces of Hg^{2+} and Pb^{2+} in real water samples. The ICP-MS instrument was equipped with a PE-AS91 auto-sampler. Samples were introduced via a cross-flow nebulizer with a Scott-type spray chamber. The NexION^{TM} 350X, auto-sampler, and peristaltic pump were controlled by the NexION^{TM} 350X Windows NT software and were fully automated.

3. Results and Discussion

3.1. Design Strategy of the Aptasensor

The strategy in this study (illustrated in Figure 1) relied on the principle that the aptamers could act as chelating factor for the analytes and undergo conformational changes that lead to changes in the electrochemical properties of aptamers containing the redox label [32]. The conformation anti-Hg aptamer turns to a hair-pin structure accommodating several Hg^{2+} ions due to T-Hg-T interaction while anti-Pb aptamer forms G-quadruplex, accommodating Pb^{2+} ion due to G-Pb-G interaction. In both cases, the redox labels come closer to the electrode surface and increase the electron transfer. The increase in concentration of target analyte can increase the concentration of coiled aptamers on the surface and subsequently increase the electrochemical current.

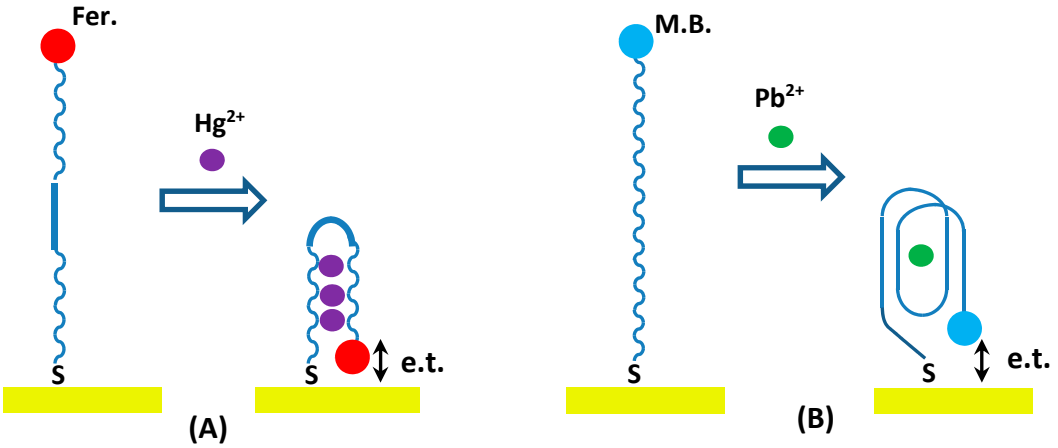

Figure 1. Schematic diagram of electrochemical detection of heavy metal ions Hg^{2+} (**A**) and Pb^{2+} (**B**) using redox-labelled aptamers.

The screen-printed gold electrodes activated with the anti-Hg^{2+} or anti-Pb^{2+} aptamers were prepared as described in the Experimental Methodology section. These electrodes, functionalized with Hg^{2+} and Pb^{2+}-specific aptamers, were used either directly as apta-sensors or stored submerged in HBB at 4 °C or room temperature for several days without any decrease in sensitivity.

3.2. Cyclic Electrochemical Measurements

Typical cyclic voltammograms (CVs) recorded on electrodes with immobilized aptamers in PBB solution with added heavy metal salts in different concentrations are shown in Figure 2. The anti-Hg^{2+} aptamer with ferrocene redox group showed well-resolved anodic and cathodic current peaks at about +0.2 V and −0.2 V, respectively, corresponding to oxidation and reduction of ferrocene (see Figure 2A). There was a clear correlation between the amplitudes of the two peaks and the concentrations of $HgCl_2$ in the buffer solution; the current rose with the increase in Hg^{2+} ions contents, as demonstrated in the schematic diagram in Figure 1. Similar results were observed for anti-Pb^{2+} aptamer labeled with methylene blue (shown in Figure 2B); however, the current peaks were not as pronounced but rather appeared as shoulders at potentials of about ±0.2 V. Again, a correlation between the values of current and $PbCl_2$ salt concentration was apparent and demonstrated the apta-sensing concept in Figure 1. Notably, the measurements on samples with immobilized aptamers stored for two to three weeks in the refrigerator (at 4 °C) yielded the same result as freshly deposited aptamers. The stored samples needed re-activation by a heating/cooling cycle in PCR unit before use. The series of CVs of samples with immobilized aptamers stored in the refrigerator for two to three weeks shown in Figure S1 as supplementary material exhibited no principle differences with the CVs recorded on freshly prepared aptamers (shown in Figure 2); however, the absolute values of the current differed amongst the samples.

Control experiments were carried out on samples without immobilized aptamers. The CV curves presented in Figure 3 showed much larger currents without characteristic peaks when compared with the samples with aptamers, which clearly indicate that the aptamer layer acts as an insulator. The observed current is due to electrochemical processes occurring in the buffer solution. The current increases with the increase in concentrations of both $HgCl_2$ and $PbCl_2$ salts.

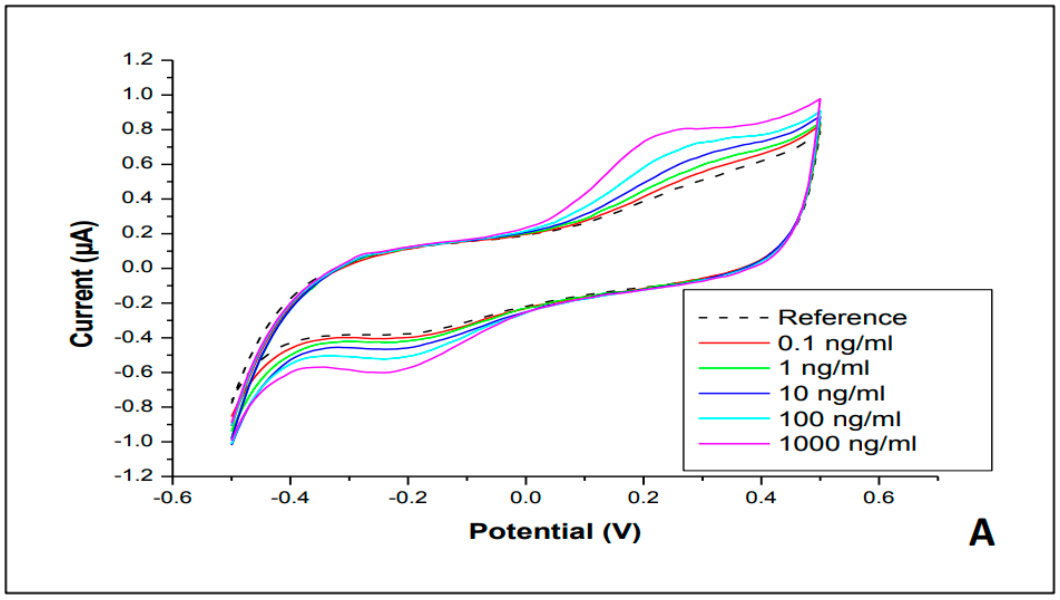

Figure 2. *Cont.*

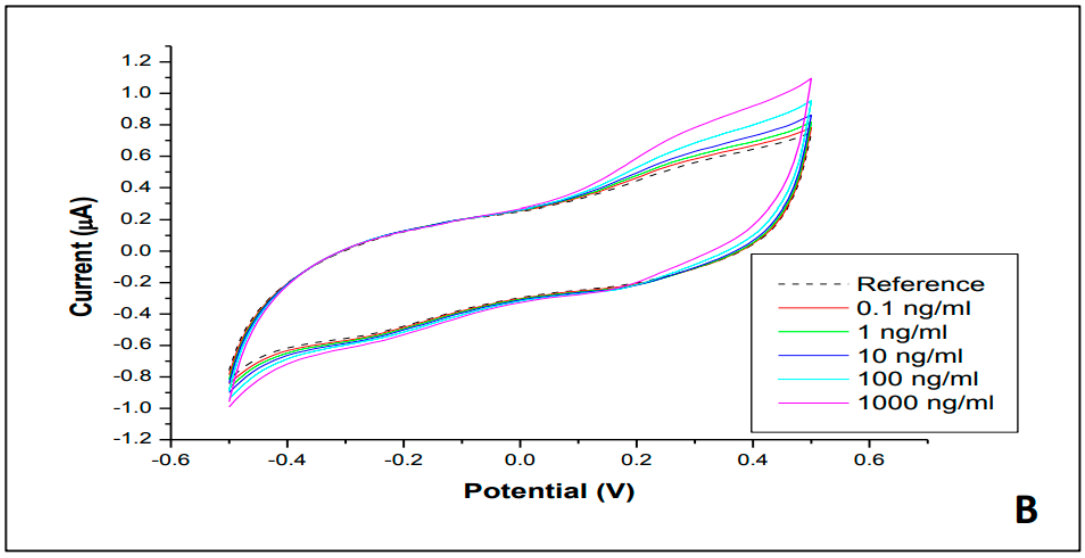

Figure 2. Cyclic voltammograms of screen-printed electrodes with immobilized anti Hg^{2+} (**A**) and anti-Pb^{2+} (**B**) aptamers in HBB solutions with different concentrations of $HgCl_2$ and $PbCl_2$ salts. The reference curves were recorded in pure HBB without heavy metal salts added.

The dependence of the anodic current changes $\Delta I_a = \left| I_a - I_{a\ ref} \right|$ at +0.2 V against the concentrations of heavy metals ions are shown in Figure 4. Therefore, the effect of background currents (I_{ref}) caused by the conductivity of HBB with added heavy metal salts was eliminated. The semi-logarithmic calibration graphs of both sensors in Figure 4 showed monotonic increase of the response in a wide range of concentrations from 0.1 to 1000 ng/mL.

The cross-sensitivity tests were carried out by measuring CV curves on samples with immobilized anti-Hg and anti-Pb aptamers to other metal (e.g., Zn, Cu, Cd, and Pb or Hg) chloride salts. The results of such tests presented in Figure 5 showed no responses for non-complementary metals, which confirm high specificity of the aptamers used.

The real samples of water taken from different natural resources in the area were tested by CV measurements on screen-printed electrodes with immobilized anti-Hg and anti-Pb aptamers. The results were arranged on the respective calibration graphs in Figure 4. For the sake of evaluation of Hg and Pb content in these samples, the concentration dependences in Figure 4 were extrapolated to lower concentrations of Hg and Pb ions below the 0.01 ng/mL level. The estimated values for Hg and Pb contents are shown near respective data points. The obtained data for real samples of water are compared in Table 1, with the results of ICP-MS testing of the same water samples. The correlation between the two sets of data is present in terms of the order of increased concentration; however, the ICP-MS values were typically three to 10 times larger than those obtained with CVs.

Table 1. ICP-MS testing results of real samples.

Sample Number	Hg^{2+} Ions (ng/mL)		Pb^{2+} Ions (ng/mL)	
	CV Results	ICP-MS Result	CV Results	ICP-MS Result
Sample 1	0.00035	0.0017	0.00009	0.0001
Sample 2	0.0013	0.0106	0.0006	0.0088
Sample 3	0.016	0.078	0.005	0.034
Sample 4	0.08	0.7	0.095	0.96
Sample 5	0.7	0.9	0.7	1.7

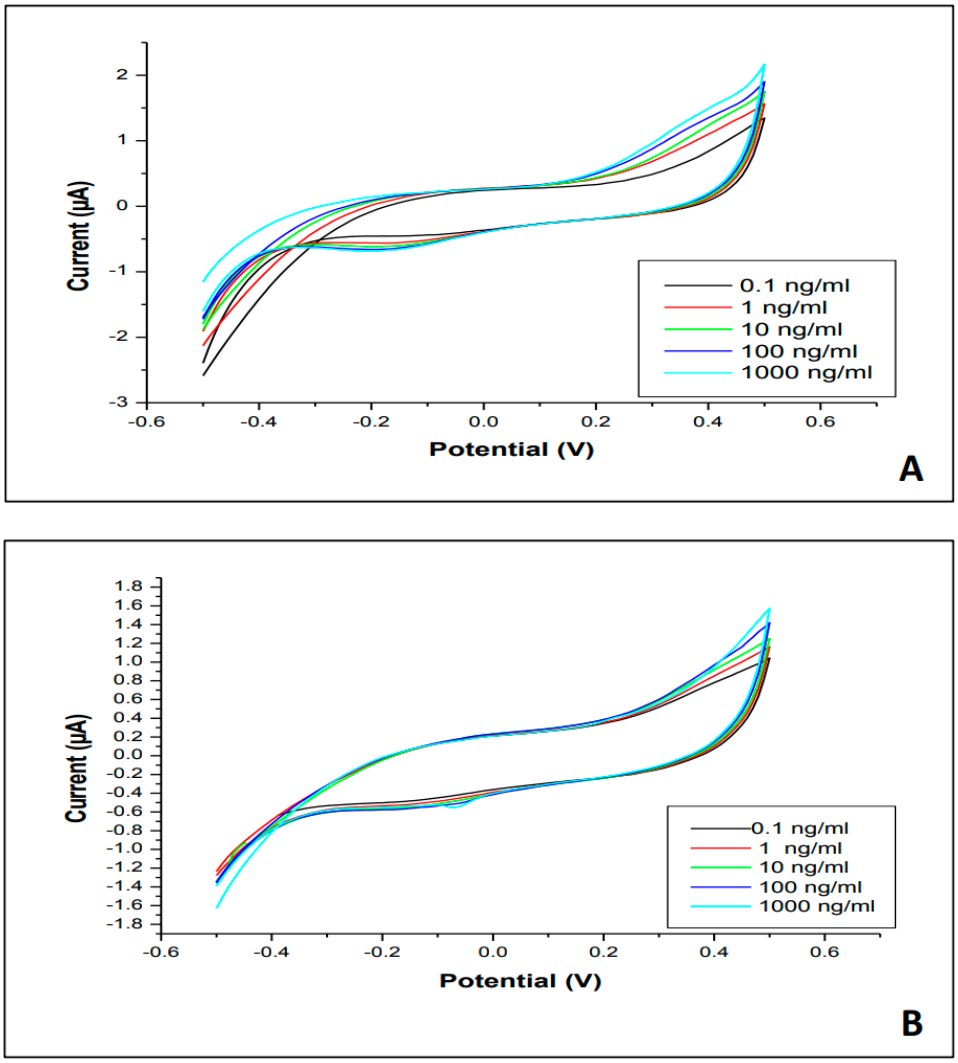

Figure 3. Cyclic voltammograms of screen-printed electrodes without immobilized aptamers in HBB solutions with different concentrations of $HgCl_2$ (**A**) and $PbCl_2$ salts (**B**).

The observed differences between CV and ICP-MS data could be attributable to several causes. Firstly, some of the samples of very clean water used in this study showed the content of Hg, and particularly Pb, below the calibration limit; accordingly, the concentrations of Hg and Pb ions can be only roughly estimated. Secondly, the methodology of testing samples of water with low contents of heavy metals was not developed properly. The choice of bottled drinking water as a reference might not be suitable. Concurrently, aptamers are known to lose their secondary structure in clear water with no $MgCl_2$ stabilizer, which might have produced wrong responses.

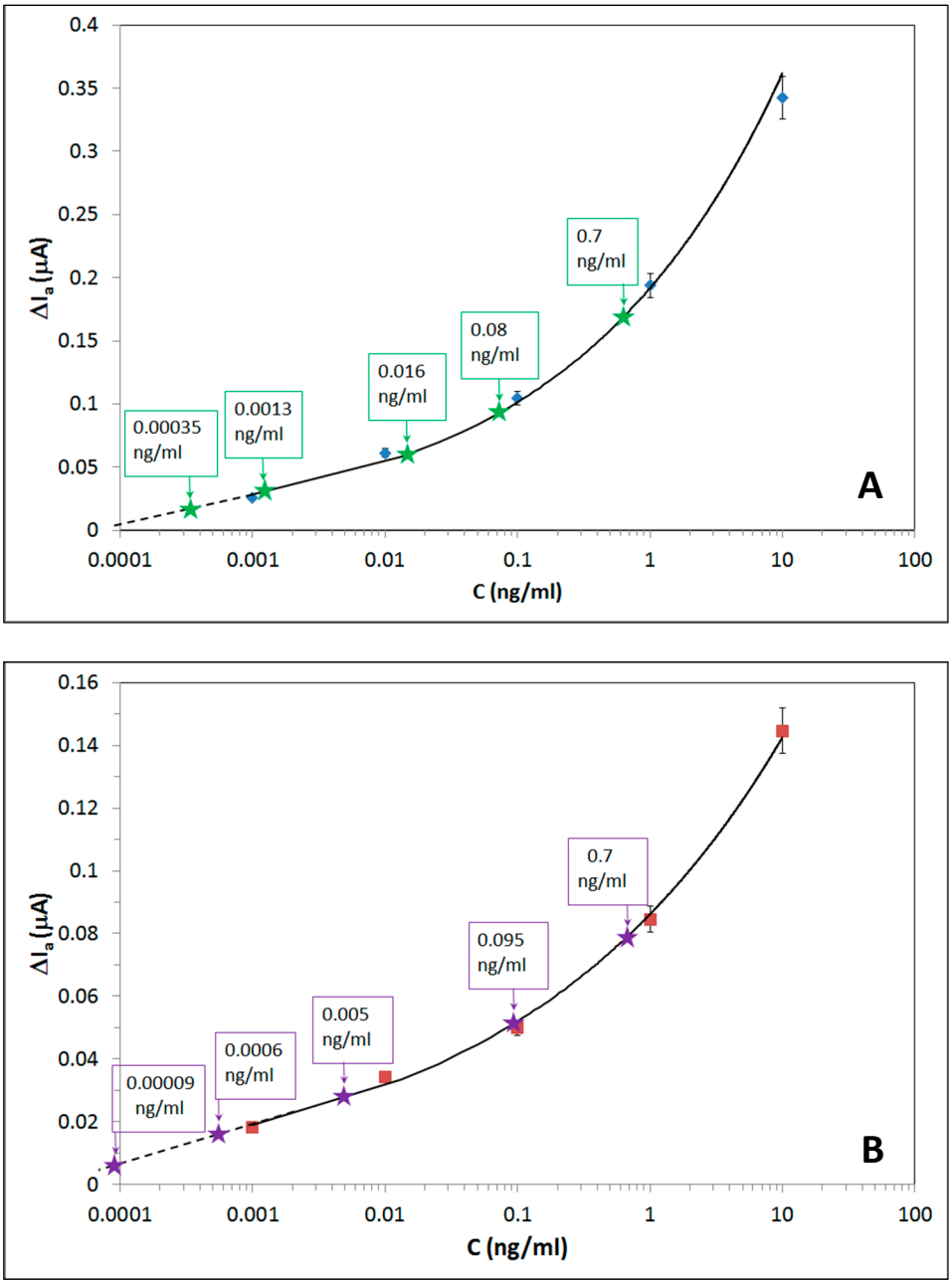

Figure 4. The concentration dependences of changes in anodic current at 0.2 V upon binding of Hg^{2+} (**A**) and Pb^{2+} (**B**) ions to respective aptamers. The star points correspond to real sample data; the concentration values are given next to those points.

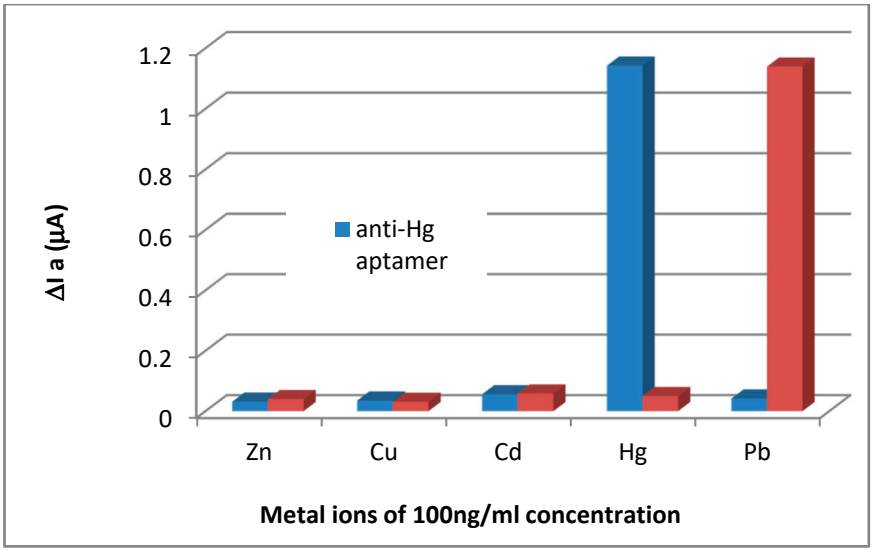

Figure 5. The cross-sensitivity tests: responses of anti-Hg^{2+} aptamer (blue) and anti-Pb^{2+} aptamer (red) to Zn^{2+}, Cu^{2+}, Cd^{2+}, Hg^{2+}, and Pb^{2+} ions in 100 ng/mL concentrations.

3.3. Impedance Spectroscopy Measurements

The impedance spectroscopy scans were carried out on interdigitated electrodes with immobilized aptamers (as well as on bare electrodes) in HBB solutions containing heavy metal salts. Typical results are shown as Nyquist plots in Figure 6. Notably, there is a major difference between these two graphs; in the presence of aptamers, the Nyquist plots in Figure 6A shift to the left and reduce in radius. This indicates the decrease in the charge transfer resistance (R_{ct}) of the surface layer with an increase in Hg^{2+} concentration; however, in the absence of aptamers, the Nyquist plots in Figure 6B remain almost unchanged, with a small decrease in the radius due to changes in the bulk resistivity of the solution. Also, the nearly perfect circular shape of Nyquist curves indicates the absence of a diffusion limitation of the charge transfer on the electrodes, an obvious result given a very small thickness of aptamer layer was in the range of a few nanometres.

The analysis of impedance spectra using an equivalent circuit model (shown as inset in Figure 6A) was carried out. According to the simplified impedance circuit model (when the diffusion impedance Z_{diff} is neglected) [33,34], the part of the impedance at critical points of the Nyquist plot are given as:

$$Z_{re} = R_b + R_{ct} \text{ at } \omega = 0 \text{ and } Z_{re} = R_b \text{ at } \omega = \infty, \quad (1)$$

where R_b is the bulk resistance of the electrolyte solution, R_{ct} and C_{dl} connected in parallel are, respectively, the charge transfer resistance and capacitance associated with an electrical charge double layer on the surface of gold electrodes.

As seen in Figure 6, the value of R_b is very small (typically in single Ohms), while R_{ct} is much larger (above 900 Ω at low concentrations of heavy metals) and decreases upon an increasing concentration of Hg^{2+} ions, likely the result of an enhancement of the electron transfer between the ferrocene label and the electrode, in line with the scheme shown in Figure 1. Concurrently, the increase of Hg^{2+} concentration without aptamers immobilized on the surface does not show any significant effect on the R_{ct} values, which corresponds well to the data presented in Figure 3.

Similar results were observed for interdigitated electrodes with immobilized anti-Pb^{2+} aptamers in solutions containing $PbCl_2$.

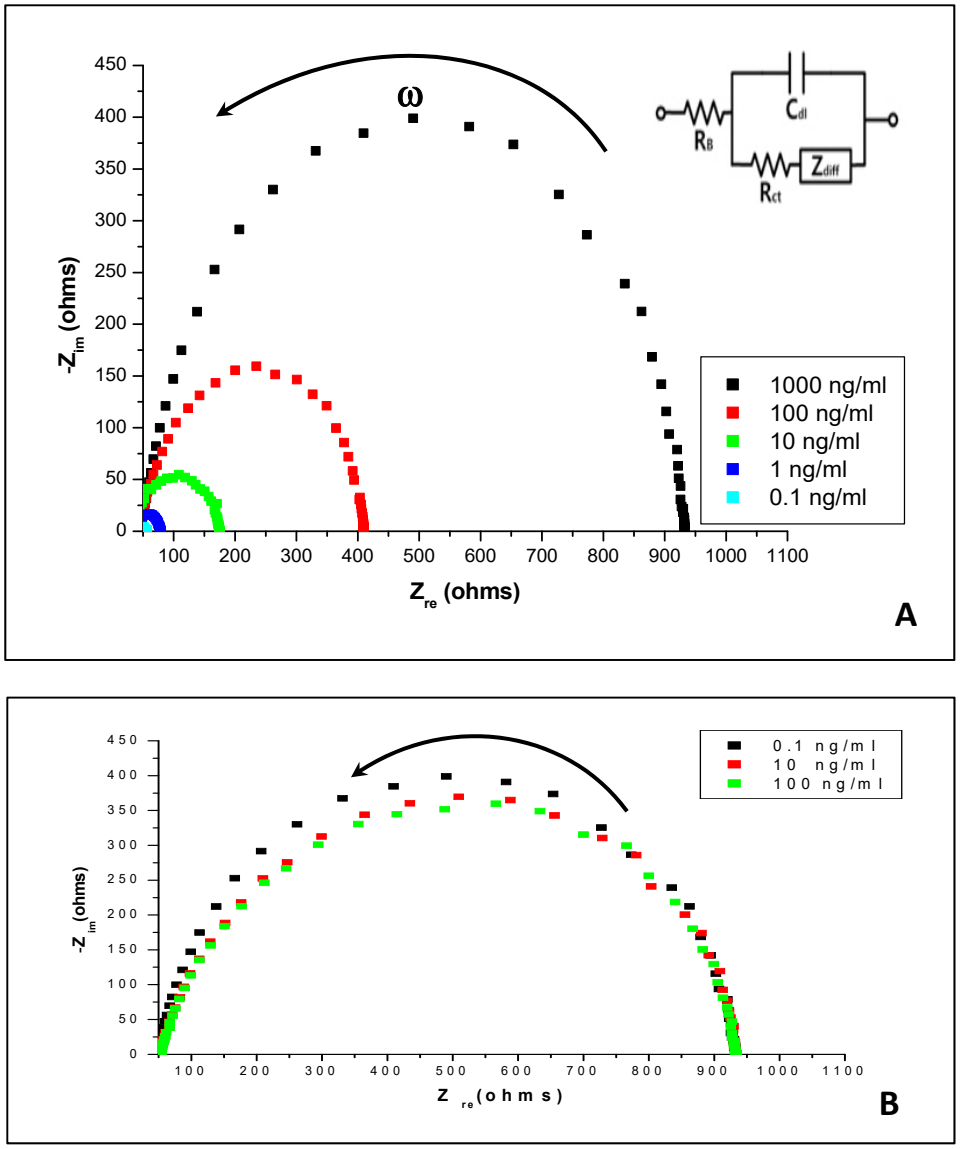

Figure 6. The Nyquist plots ($-Z_{im}$ vs. Z_{re}) for interdigitated electrodes with immobilized anti-Hg^{2+} aptamers binding Hg^{2+} ions of different concentrations (**A**); the Nyquist plot for bare interdigitated electrodes in solutions with different concentrations of $HgCl_2$ (**B**).

3.4. The Kinetics of Aptamers (Hg^{2+} and Pb^{2+}) Binding

The kinetics of Hg^{2+} and Pb^{2+} ions binding to specific aptamers were studied by recording the time dependencies of cathodic current (at −0.2 V) of three-electrode assemblies with immobilized aptamers for different concentrations of both metals ions. Cathodic current was chosen because of a smaller shift of the reduction peak upon binding Hg^{2+} ions. Typical time dependences for anti-Hg^{2+} aptamers are shown in Figure 7 for different concentrations of $HgCl_2$ salt varied from 0.01 ng/mL to 1 mg/mL. Then, the characteristic time constants (τ) were evaluated for every concentration of Hg^{2+} by fitting the respective kinetics curves to rising exponential function. The resulted dependence of $1/\tau$ versus the concentration (C) of Hg^{2+} ions is shown in Figure 7 as an inset.

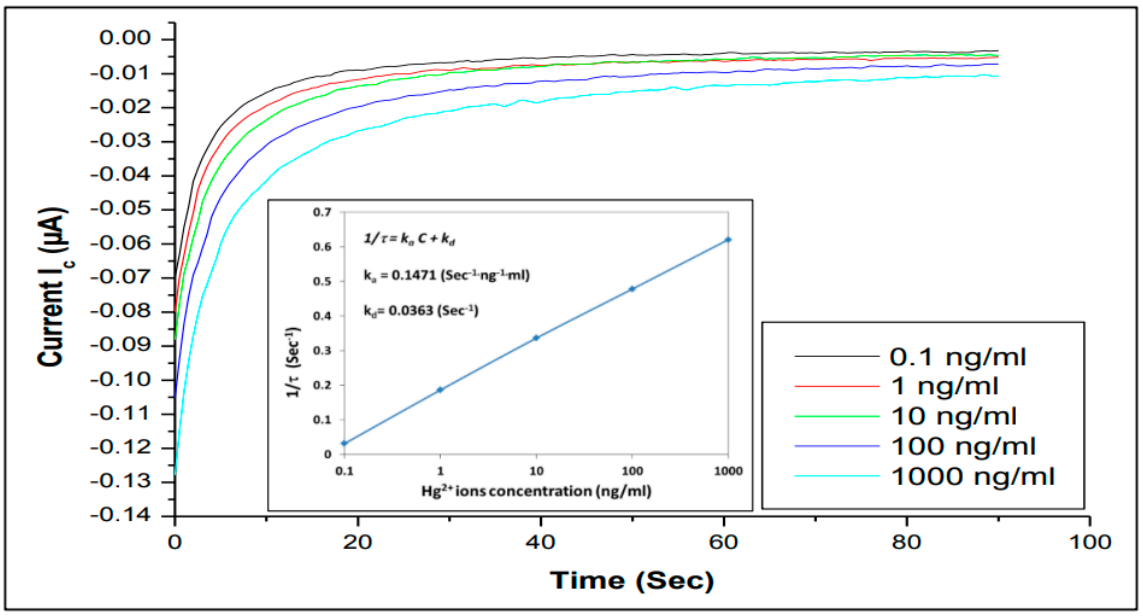

Figure 7. Time dependencies of the cathode current at fixed voltage of −0.2 V for different concentrations of different concentrations Hg^{2+} binding to anti-Hg^{2+} aptamer. The inset shows the dependence of $1/\tau$ against the concentration of Hg^{2+} ions.

Following the Langmuir adsorption law, the reciprocal time constant ($1/\tau$) depends on the analyte adsorption and desorption rates (k_a and k_d) as well as the concentration (C) of analytes (in our case, Hg^{2+} and Pb^{2+}) as:

$$1/\tau = k_a C + k_d \quad (2)$$

The values of k_a and k_d can be found, respectively, as the gradient and intercept of the linear dependence $1/\tau$ against C. Then, both the association constant (K_A) and affinity constant (K_D) can be found as $K_A = k_a/k_d$ and $K_D = 1/K_A$ [35,36].

The values of k_a and k_d were calculated as: $k_a = 0.1471(\text{sec}^{-1}\cdot\text{ng}^{-1}\cdot\text{mL}) \times 271.52(\text{g}\cdot\text{mol}^{-1}) \times 10^3\ (\text{mL}\cdot\text{ng}^{-1}) \approx 3.94.104\ (\text{sec}^{-1}\cdot\text{mol}^{-1})$ and $k_d = 0.0363\ (\text{sec}^{-1})$, where 271.52 ($\text{g}\cdot\text{mol}^{-1}$) is molecular weight of $HgCl_2$, and 10^3 factor was used as conversion from ng/mL to μg/mL. Therefore, $K_A = k_a/k_d = 1.1 \times 10^6\ (\text{mol}^{-1})$ and $K_D = 9.08 \times 10^{-7}$ (mol) for anti-Hg^{2+}aptamer.

A similar analysis was carried out for binding kinetics of anti-Pb^{2+} aptamer, and quite similar values of $K_A = 1.2 \times 10^6\ (\text{mol}^{-1})$ and $K_D = 8.5534 \times 10^{-7}$ (mol) were found.

The obtained K_A and K_D values for both anti-Hg^{2+} and anti-Pb^{2+} aptamers correspond well to the aptamers affinity evaluated in the process of their synthesis [37,38], and they are typical for highly specific binding reactions of analytes to aptamers or antibodies.

4. Conclusions and Future Work

The concept of electrochemical apta-sensor for heavy metal ions was proved, and the results obtained were encouraging. The selectivity and sensitivity of this apta-sensor to heavy metals ions, e.g., Hg^{2+} and Pb^{2+}, is high and thus promising for the development of novel, simple, and cost-effective electrochemical apta-sensors for rapid detection of heavy metals in water.

A series of cyclic voltammogramm and impedance spectroscopy measurements allowed the investigation of the mechanism of aptamer/heavy metal binding. The proposed model electrochemical apta-sensing, based on changing the conformation of the aptamer oligonucleotide chain from a linear to a folded one, thus bringing the redox label closer to metal surface and increasing the electron charge transfer, was proved. A simple detection of anodic (or cathodic) current at fixed voltage corresponding to oxidation (or reduction) peak potential is sufficient for detection of Hg^{2+} and Pb^{2+} in a wide range of concentrations, as low as 0.1 ng/mL (or 0.1 ppb). The detection of heavy metals in real water

samples was attempted and was partially successful; however, further work is required for developing methodology of real samples testing.

The study of aptamer/target binding kinetics yielded the values for the association constant $K_A = 1.1 \times 10^6$ (mol^{-1}) and the affinity constant $K_D = 9.08 \times 10^{-7}$ (mol) for aptamer/Hg^{2+} binding; similar values of the association constant $K_A = 1.2 \times 10^6$ (mol^{-1}) and the affinity constant $K_D = 8.33 \times 10^{-7}$ (mol) were found for aptamer/Pb^{2+} binding. This study proved highly specific interaction between heavy metal ions and their specific aptamers.

Further work could focus on development of the apta-sensor array for detection of other heavy metals (chromium, cadmium, arsenic, nickel, copper, silver, zinc, etc.) using simple DC electrochemical transducers. The different redox-labels can be used in future for simultaneous detection of different heavy metals.

Supplementary Materials: The following are available online at http://www.mdpi.com/2227-9040/7/2/27/s1, Figure S1. The series of CVs of samples with immobilized aptamers stored in the fridge for two to three week.

Author Contributions: H.A. (experimental work, data analysis, and writing), A.N. (supervision, data analysis, writing), T.J.S. (supervision, aptamer assay, discussion of results).

Acknowledgments: One of the authors would like to thank the Iraqi Government, Ministry of Higher Education and Scientific Research, and the University of Basrah for sponsoring and supporting the PhD project and this research.

Conflicts of Interest: The authors declare no conflict of interest.

References

1. Förstner, U.; Wittmann, G.T. *Metal Pollution in the Aquatic Environment*; Springer Science & Business Media: Berlin/Heidelberg, Germany, 2012.
2. Abu-Ali, H.; Nabok, A.; Smith, T.; Al-Shanawa, M. Inhibition Biosensor Based on DC and AC Electrical Measurements of Bacteria Samples. *Proc. Technol.* **2017**, *27*, 129–130. [CrossRef]
3. Duruibe, J.O.; Ogwuegbu, M.O.C.; Egwurugwu, J.N. Heavy metal pollution and human biotoxic effects. *Int. J. Phys. Sci.* **2007**, *2*, 112–118.
4. Clarkson, T.W.; Magos, L.; Myers, G.J. The toxicology of mercury current exposures and clinical manifestations. *N. Eng. J. Med.* **2003**, *349*, 1731–1737. [CrossRef] [PubMed]
5. Saidur, M.R.; Aziz, A.A.; Basirun, W.J. Recent advances in DNA-based electrochemical biosensors for heavy metal ion detection: A review. *Biosens. Bioelectron.* **2017**, *90*, 125–139. [CrossRef] [PubMed]
6. Parisi, L.; Galli, C.; Neri, A.; Toffoli, A.; Calciolari, E.; Manfredi, E.; Macaluso, C. Aptamers improve the bioactivity of biomaterials. *Aptamers* **2017**, *1*, 3–12.
7. Wang, J.; Wu, C.; Hu, N.; Zhou, J.; Du, L.; Wang, P. Micro-fabricated electrochemical cell-based biosensors for analysis of living cells in vitro. *Biosensors* **2012**, *2*, 127–170. [CrossRef]
8. Tan, F.; Cong, L.; Saucedo, N.M.; Gao, J.; Li, X.; Mulchandani, A. An electrochemically reduced graphene oxide chemiresistive sensor for sensitive detection of Hg^{2+} ion in water samples. *J. Hazard. Mater.* **2016**, *320*, 226–233. [CrossRef]
9. Abu-Ali, H.; Nabok, A.; Smith, T.; Al-Shanawa, M. Development of electrochemical inhibition biosensor based on bacteria for detection of environmental pollutants. *Sens. Bio-Sens. Res.* **2017**, *13*, 109–114. [CrossRef]
10. Ben-Yoav, H.; Almog, R.O.; Sverdlov, Y.; Sternheim, M.; Belkin, S.; Freeman, A.; Shacham-Diamand, Y. Modified working electrodes for electrochemical whole-cell microchips. *Electrochim. Acta* **2012**, *82*, 109–114. [CrossRef]
11. Belkin, S.; Gu, M.B. *Whole Cell Sensing Systems I*; Reporter Cells and Devices; Springer: Berlin/Heidelberg, Germany, 2010; p. 220.
12. Citartan, M.; Gopinath, S.C.; Tominaga, J.; Tan, S.C.; Tang, T.H. Assays for aptamer-based platforms. *Biosens. Bioelectron.* **2012**, *34*, 1–11. [CrossRef]
13. Ferapontova, E.E.; Olsen, E.M.; Gothelf, K.V. An RNA aptamer-based electrochemical biosensor for detection of theophylline in serum. *J. Am. Chem. Soc.* **2008**, *130*, 4256–4258. [CrossRef] [PubMed]
14. He, J.; Liu, Y.; Fan, M.; Liu, X. Isolation and identification of the DNA aptamer target to acetamiprid. *J. Agric. Food Chem.* **2011**, *59*, 1582–1586. [CrossRef] [PubMed]

15. Al Rubaye, A.; Nabok, A.; Catanante, G.; Marty, J.L.; Takacs, E.; Szekacs, A. Detection of ochratoxin A in aptamer assay using total internal reflection ellipsometry. *Sens. Actuators B Chem.* **2018**, *263*, 248–251. [CrossRef]
16. Zhang, W.; Liu, Q.; Guo, Z.; Lin, J. Practical application of aptamer-based biosensors in detection of low molecular weight pollutants in water sources. *Molecules* **2018**, *23*, 344. [CrossRef] [PubMed]
17. Sassolas, A.; Blum, L.J.; Leca-Bouvier, B.D. Optical detection systems using immobilized aptamers. *Biosens. Bioelectron* **2011**, *26*, 3725–3736. [CrossRef] [PubMed]
18. Hamula, C.L.; Guthrie, J.W.; Zhang, H.; Li, X.F.; Le, X.C. Selection and analytical applications of aptamers. *Trends Anal. Chem.* **2006**, *25*, 681–691. [CrossRef]
19. Chen, L.; Cai, Q.; Luo, F.; Chen, X.; Zhu, X.; Qiu, B.; Chen, G. A sensitive aptasensor for adenosine based on the quenching of Ru (bpy)$^{32+}$-doped silica nanoparticle ECL by ferrocene. *Chem. Commun.* **2010**, *46*, 7751–7753. [CrossRef]
20. Yang, L.; Fung, C.W.; Cho, E.J.; Ellington, A.D. Real-time rolling circle amplification for protein detection. *Anal. Chem.* **2007**, *79*, 3320–3329. [CrossRef]
21. Patolsky, F.; Weizmann, Y.; Willner, I. Redox-active nucleic-acid replica for the amplified bioelectrocatalytic detection of viral DNA. *J. Am. Chem. Soc.* **2002**, *124*, 770–772. [CrossRef]
22. Deng, C.; Chen, J.; Nie, L.; Nie, Z.; Yao, S. Sensitive bifunctional aptamer-based electrochemical biosensor for small molecules and protein. *Anal. Chem.* **2009**, *81*, 9972–9978. [CrossRef]
23. Li, T.; Dong, S.; Wang, E. Label-free colorimetric detection of aqueous mercury ion using Hg^{2+}-modulated G-quadruplex-based DNAzymes. *Anal. Chem.* **2009**, *81*, 2144–2149. [CrossRef] [PubMed]
24. Barthelmebs, L.; Hayat, A.; Limiadi, A.W.; Marty, J.L.; Noguer, T. Electrochemical DNA aptamer-based biosensor for OTA detection, using superparamagnetic nanoparticles. *Sens. Actuators B Chem.* **2011**, *156*, 932–937. [CrossRef]
25. Zeng, G.; Zhang, C.; Huang, D.; Lai, C.; Tang, L.; Zhou, Y.; Xu, P.; Wang, H.; Qin, L.; Cheng, M. Practical and re-generable electrochemical aptasensor based on nanoporous gold and thymine-Hg^{2+}-thymine base pairs for Hg^{2+} detection. *Biosens. Bioelectron.* **2017**, *90*, 542–548. [CrossRef] [PubMed]
26. Zhang, Y.; Yuan, Q.; Chen, T.; Zhang, X.; Chen, Y.; Tan, W. DNA-capped mesoporous silica nanoparticles as an ion-responsive release system to determine the presence of mercury in aqueous solutions. *Anal. Chem.* **2012**, *84*, 1956–1962. [CrossRef] [PubMed]
27. An, J.H.; Park, S.J.; Kwon, O.S.; Bae, J.; Jang, J. High-performance flexible graphene aptasensor for mercury detection in mussels. *ACS Nano* **2013**, *7*, 10563–10571. [CrossRef] [PubMed]
28. Gao, F.; Gao, C.; He, S.; Wang, Q.; Wu, A. Label-free electrochemical lead (II) aptasensor using thionine as the signalling molecule and graphene as signal-enhancing platform. *Biosens. Bioelectron.* **2016**, *81*, 15–22. [CrossRef]
29. Dolati, S.; Ramezani, M.; Abnous, K.; Taghdisi, S.M. Recent nucleic acid based biosensors for Pb^{2+} detection. *Sens. Actuators B Chem.* **2017**, *246*, 864–878. [CrossRef]
30. Wang, S.E.; Si, S. Aptamer biosensing platform based on carbon nanotube long-range energy transfer for sensitive, selective and multicolour fluorescent heavy metal ion analysis. *Anal. Methods* **2013**, *5*, 2947–2953. [CrossRef]
31. Cui, L.; Wu, J.; Ju, H. Label-free signal-on aptasensor for sensitive electrochemical detection of arsenite. *Biosens. Bioelectron.* **2016**, *79*, 861–865. [CrossRef]
32. Rhouati, A.; Yang, C.; Hayat, A.; Marty, J.-L. Aptamers: A promising tool for ochratoxin A detection in food analysis. *Toxins* **2013**, *5*, 1988–2008. [CrossRef] [PubMed]
33. Macdonald, J.R. Impedance spectroscopy. *Ann. Biomed. Eng.* **1992**, *20*, 289–305. [CrossRef] [PubMed]
34. Karlsson, R.; Michaelsson, A.; Mattsson, L. Kinetic analysis of monoclonal antibody-antigen interactions with a new biosensor based analytical system. *J. Immunol. Methods* **1991**, *145*, 229–240. [CrossRef]
35. Battaglioli, G.; Liu, H.; Martin, D.L. Kinetic differences between the isoforms of glutamate decarboxylase: Implications for the regulation of GABA synthesis. *J. Neurochem.* **2003**, *86*, 879–887. [CrossRef] [PubMed]
36. Nabok, A.; Tsargorodskaya, A.; Mustafa, M.K.; Szekacs, I.; Starodub, N.F.; Szekacs, A. Detection of low molecular weight toxins using an optical phase method of ellipsometry. *Sens. Actuators B Chem.* **2011**, *154*, 232–237. [CrossRef]

37. Wang, Y.; Zheng, Y.; Yang, F.; Yang, X. Dual polarisation interferometry for real-time, label-free detection of interaction of mercury (II) with mercury-specific oligonucleotides. *Chem. Commun.* **2012**, *48*, 2873–2875. [CrossRef]
38. Kim, H.N.; Ren, W.X.; Kim, J.S.; Yoon, J. Fluorescent and colorimetric sensors for detection of lead, cadmium, and mercury ions. *Chem. Soc. Rev.* **2012**, *41*, 3210–3244. [CrossRef] [PubMed]